TWO SURFACE-TENSION FORMULATIONS FOR THE LEVEL SET INTERFACE-TRACKING METHOD

S.V. Shepel, B.L. Smith

The paper describes a comparative study of two surface-tension models for the Level Set interface-tracking method. In both models, the surface tension is represented as a body force, concentrated near the interface, but the technical implementation of the two options is different. The first is based on a traditional Level Set approach, in which the surface tension is distributed over a narrow band around the interface using a smoothed Delta function. In the second model, which is based on the integral form of the fluid-flow equations, the force is imposed only in those computational cells through which the interface passes. Both models have been incorporated into the Finite-Element/Finite-Volume Level Set method, previously implemented into the commercial Computational Fluid Dynamics (CFD) code CFX-4. A critical evaluation of the two models, undertaken in the context of four standard Level Set benchmark problems, shows that the first model, based on the smoothed Delta function approach, is the more general, and more robust, of the two.

1 INTRODUCTION

The work reported here concerns the modelling of viscous, incompressible, two-phase flows in which the phases are separated by a distinct interface. Existing computational methods for solving such problems include the Front-Tracking Method [1], the Boundary Integral Method [2], the Phase-Field Method [3], the Second Gradient Method [4], the Volume-of-Fluid (VOF) Method [5], and the Level Set (LS) Method [6]. Here, we focus on recent developments of the Level Set method, which we have implemented into the commercial code CFX-4 . The relative strengths of the Level Set approach, vis-à-vis the other interface-tracking methods, lie in its ability to accurately represent flows in which surface-tension forces dominate, and those for which there are abrupt changes in topology.

In CFX-4, the Navier-Stokes equations governing the fluid flow are solved in conservative form, using the Finite-Volume (FV) method. The code employs structured, body-fitted grids, made up of hexahedral computational cells. The Level Set interface-tracking equations, however, are generally not written in conservative form [6], and consequently cannot be handled using the FV method.

Since we are interested in modelling industrial interfacial flows, in both two and three dimensions, and using structured and/or unstructured grids, we have chosen the FE Streamline-Upwind/Petrov-Galerkin (SUPG) method for solving the Level Set equations. This method is second-order accurate, robust, and readily adjustable to 3-D, unstructured grids [7]. Consequently, we refer herein to this combination of non-conservative FE and conservative FV methods for solving the interface-tracking and fluid-flow equations, respectively, as a *mixed FE-FV formulation*.

To our knowledge, utilisation of the conservative form of both the fluid flow and interface-tracking equations for incompressible flows has been used only once: by Sussman and Puckett [8], in the context of the coupled Level Set/VOF (CLSVOF) method. There remains a distinct lack of information for mixed formulations, i.e. those involving the conservative form of the incompressible fluid flow equations, together with non-conservative form of the interface-tracking equations. Nonetheless, the mixed formulation has certain advantages from the point of view of implementation into the framework of established commercial CFD codes, since many of them incorporate conservative FV Navier-Stokes solvers.

In the traditional Level Set method, based on the non-conservative form of the equations, the surface-tension force is generally modelled as a body force, concentrated in a narrow band around the interface.

According to this model, the force has a maximum on the interface, but decays rapidly on either side of it. Typically, the band over which the surface tension force is smoothed is pre-set to be 4 or 5 computational cells. However, Ilic *et al*. [9] have recently reported a successful application of an alternative method, based on the integral form of the fluid-flow equations. In this approach, the surface-tension force is represented only in those cells actually traversed by the interface.

Effectively then, the thickness of the band in which the surface force is modelled is reduced to just only one cell. In their paper, Ilic *et al*. have incorporated their model into a Piecewise-Linear Interface Construction (PLIC) VOF interface-tracking technique, and used it to simulate a bubble-train flow.

To our knowledge, such a model has never been used before in the context of the Level Set approach. The difficulty is that the model cannot be incorporated into the traditional Level Set formulation, since it is not generally formulated in terms of the integral form of the fluid-flow equations. However, the mixed FE-FV Level Set formulation used here is itself based on the integral form of the fluid-flow equations, and therefore a surface tension model analogous to that of Ilic *et al*. [9] can be implemented. This fact gives us a unique opportunity to critically and quantitatively assess the relative merits of “smoothed” and “concentrated” surface tension models.

2 PROBLEM FORMULATION

2.1 FE-FV Mixed Level Set Formulation

The local equations governing the motion of the unsteady, viscous, Newtonian, incompressible, isothermal, immiscible two-phase flow of a gas-liquid mixture are the Navier-Stokes equations, which in conservative form may be expressed as:

$$\frac{\partial(\rho^*\mathbf{u}^*)}{\partial t^*}+\nabla\cdot(\rho^*\mathbf{u}^*\otimes\mathbf{u}^*)=-\nabla p^*+\frac{1}{Re}\nabla\cdot(\mu^*\nabla\mathbf{u}^*)+$$

$$+\frac{\rho^*\mathbf{g}^*}{Fr}+\frac{\mathbf{B}^*_{st}}{We}, \qquad (1a)$$

$$\frac{\partial\rho^*}{\partial t^*}+\nabla\cdot(\rho^*\mathbf{u}^*)=0, \qquad (1b)$$

in which

$$\mathbf{u}^*=\mathbf{u}/u_c,\ \mathbf{x}^*=\mathbf{x}/l_c,\ t^*=tu_c/l_c,\ \mathbf{g}^*=\mathbf{g}/g \qquad (1c)$$

and

$$\rho^*=\rho/\rho_L,\ \mu^*=\mu/\mu_L,\ p^*=p/\rho_L u_c^2,\ \mathbf{B}^*_{\mathrm{st}}=\mathbf{B}_{\mathrm{st}}\,l_c^2/\sigma.$$

The equations are written in dimensionless form, the asterisk indicating dimensionless variables, adopting the scaling laws indicated.

In these equations, $\mathbf{u}$ is the velocity vector, $\mathbf{x}$ is the distance, t the time, $\mathbf{g}$ the acceleration of gravity, ρ the density, μ the dynamic viscosity, p the pressure, and $\mathbf{B}_{\mathrm{st}}$ the surface-tension force. Correspondingly, u_c and l_c are characteristic velocity and distance scales, and σ the surface tension. Here, and later, the subscripts *L* and *G* denote values corresponding to the liquid and gas phases, respectively.

The following dimensionless groups appear in Eqs. (1):

$$Re=\rho_L u_c l_c/\mu_L,\ Fr=u_c^2/gl_c,\ We=\rho_L u_c^2 l_c/\sigma, \qquad (2)$$

which are, respectively, the Reynolds, Froude and Weber numbers for the flow.

The interface between the two phases is represented by a continuous scalar function $\phi(\mathbf{x},t)$, which is negative in the liquid phase and positive in the gas phase. On the interface, therefore, the function takes the value zero, so that the location of the physical interface between the phases is associated with the mathematical surface $\phi(\mathbf{x},t)=0$. The function ϕ is called the Level Set function, and is typically defined as the signed distance to the interface. Correspondingly, we set $\phi=-d(\mathbf{x},t)$ if $\mathbf{x}$ lies in the liquid, and $\phi=+d(\mathbf{x},t)$ if $\mathbf{x}$ lies in the gas, where $d(\mathbf{x},t)$ is the shortest distance from the point $\mathbf{x}$ to the interface. Since the interface moves with the flow, the evolution of ϕ is governed by the advection equation:

$$\frac{\partial\phi^*}{\partial t^*}+\mathbf{u}^*\cdot\nabla\phi^*=0, \qquad (3)$$

in which $\phi^*=\phi/l_c$ is the dimensionless equivalent of the Level Set function.

In the Level Set method, the density and viscosity of the fluid are typically interpolated across the interface, in order to allow a smooth transition in properties from one phase to the other:

$$\rho(\mathbf{x},t)=\rho_L+(\rho_G-\rho_L)\,H_\varepsilon(\phi(\mathbf{x},t)), \qquad (4a)$$

$$\mu(\mathbf{x},t)=\mu_L+(\mu_G-\mu_L)\,H_\varepsilon(\phi(\mathbf{x},t)), \qquad (4b)$$

where $H_\varepsilon(\phi)$ is a smoothed Heaviside function, which is used instead of the discontinuous function to aid numerical stability.

Following the work of Sussman *et al.* [10], we use the following expression for $H_\varepsilon(\phi)$:

$$H_\varepsilon(\phi)=\begin{cases}0 & \text{if } \phi<-\varepsilon\\ (\phi+\varepsilon)/(2\varepsilon)+\sin(\pi\phi/\varepsilon)/(2\pi) & \text{if } |\phi|\le\varepsilon\\ 1 & \text{if } \phi>\varepsilon\end{cases} \qquad (5)$$

where ε is a small parameter of the order of the size of the mesh cells close to the interface. It can be seen from Eq. (5) that the parameter ε is essentially the half-thickness of the transitional region over which the fluid properties are interpolated. In principle, it is possible to use different values of ε for density and viscosity, though in the simulations reported here both are set to the same value, $2h$, where h is the average mesh size in the region of the interface.

In the process of solving the advection Eq. (3), the Level Set function, $\phi(\mathbf{x},t)$, ceases to be the signed distance from the interface, even if it had been properly initialized at $t=0$. However, in order to interpolate the phase properties strictly according to Eqs. (4), it is necessary to keep the Level Set function equal to the signed distance function $d(\mathbf{x},t)$ at all times. Consequently, the Level Set field, $\phi(\mathbf{x},t)$, needs to be *reinitialized* at every time step. An efficient re-initialization procedure has been proposed by Sussman and Fatemi [11], based on integrating the following equation to steady-state:

$$\frac{\partial\phi^*}{\partial\tau^*}+\mathrm{sign}(\phi_0^*)\left(|\nabla\phi^*|-1\right)=\lambda\delta^*_\varepsilon(\phi^*)|\nabla\phi^*|, \qquad (6)$$

where τ^* is a time-like variable (used only to approach the steady-state solution), ϕ_0 is the initial Level Set function before re-initialization, $\delta_\varepsilon(\phi)$ is the smoothed Delta function, defined as $\delta_\varepsilon(\phi)=H'_\varepsilon(\phi)$, and λ is a correction coefficient, calculated in such a way as to ensure mass conservation up to the first-order term in the Taylor expansion of the integral

$$\partial_\tau\int_\Omega H_\varepsilon(\phi)\,d\phi$$

; details, are given in [11].

In the code CFX-4, all variables, including velocity, pressure and bulk body forces, are defined at cell centres. The boundary conditions are imposed at boundary nodes, which are located at the centres of the cell faces bordering the fluid domain. In the

SUPG FE method, however, variables are defined at element vertices. If the same mesh were to be used to solve both the fluid flow Equations (1) and the Level Set Equations (3,6), interpolation procedures would have to be invoked to transfer information from cell centres to vertices. In order to avoid this, which would inevitably result in smearing of the solution, we overlay the FV mesh by an FE mesh, whose vertices are constructed from the centres and boundary nodes of the FV mesh. In this "hybrid" approach, we use the FV mesh to solve the Navier-Stokes equations, and the FE mesh to solve the Level Set equations. The concept is illustrated in Fig. 1.

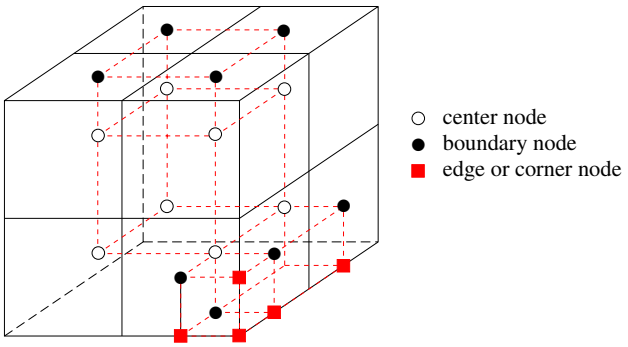

Fig. 1: Construction of the FE mesh by overlaying the FV grid: a schematic of grids, nodes and elements. The dashed lines show the edges of the finite elements.

Note that construction of the FE mesh requires the introduction of a new type of node, not present in the FV mesh. The new nodes are located on the edges and corners of the external boundaries of the fluid domain, and velocities at such nodes need to be prescribed according to the appropriate boundary conditions. The FE elements constructed this way are hexahedral in type, and isoparametric, bilinear shape functions are employed to prescribe the distribution of quantities within each element. Details of the implementation of the Level Set interface-tracking method into CFX-4 are described by Shepel *et al*. [12].

2.2 Surface-Tension Modelling

In the traditional Level Set method, as mentioned previously, the surface tension is modelled as a body force, concentrated in a narrow band around the interface [10]. According to this prescription, which we later refer to as *Method A*, the surface-tension force is defined as follows:

$$\mathbf{B}_{st} = \sigma\kappa\nabla\phi\delta_{\varepsilon}(\phi). \qquad (7)$$

Here, the function $\delta_{\varepsilon}(\phi)$ is defined in terms of ε_{σ}, the half-thickness of the band. Typically, the value $\varepsilon_{\sigma} = 2h$ is used [10,11].

The normal to the interface, and the curvature, are given by, respectively:

$$\mathbf{n} = \frac{\nabla\phi}{|\nabla\phi|} \quad , \quad \kappa = \nabla\cdot\frac{\nabla\phi}{|\nabla\phi|}. \qquad (8)$$

In contrast, in the alternative employed by Ilic et.al. [9] approach, the surface-tension force is defined at the centres of those computational cells actually crossed by the interface. In this formulation,

$$\mathbf{B}_{st} = \sigma\kappa\Gamma_{in}\mathbf{n}. \qquad (9)$$

where Γ_{in} is the interfacial area-volume ratio, defined as $\Gamma_{in} = \Delta a / \Delta V$, in which Δa is the area of the interface segment confined within the volume ΔV. In the present work, we refer to this approach as *Method B*. The difference between our work and that [9], is that they used VOF data to calculate the interface normal, $\mathbf{n}$, and curvature, κ, whereas we calculate these quantities using the Level Set function, ϕ, as given in Eq. (8).

The primary objective of the present study is to compare the relative performances of the *distributed* and *concentrated* surface-tension formulations, defined by Eq. (7) and Eq. (9), respectively. During preliminary calculations, however, for problems in which the surface-tension effects are dominant, we found that the use of Method B can lead to slow convergence, and sometimes to erroneous solutions. The principal difficulty appeared to arise from the abrupt change in surface-tension force as the gas/liquid interface moves from one computational cell to another.

To illustrate the difficulty, consider the FV cell shown in Fig. 2a. In this situation, the interface is located close to the right vertical cell edge of the left cell, and is almost parallel to it.

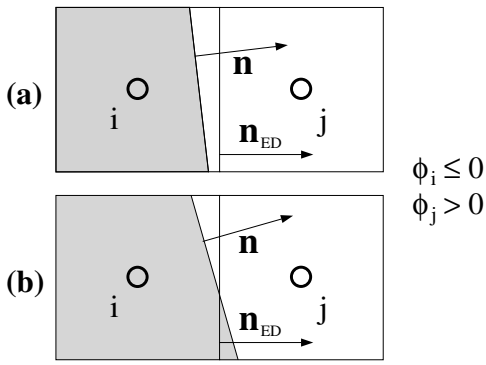

Fig. 2: Possible orientation of a phase interface; the region occupied by the liquid phase is shown in grey.

If the interface, moving to the right, crosses the entire cell edge in one time step, the surface-tension force at nodes *i* and *j*, as given by Eq. (9), changes in a discontinuous manner, which can result in poor convergence of the underlying numerical scheme, and/or lack of precision.

Thus, in order to employ Method B successfully for flows with strong surface tension effects, it is necessary to provide some means of smoothing the

surface tension distribution, $\mathbf{B}_{st}$, around the interface. We have developed a straightforward smoothing procedure that can be readily applied to rectangular grids (the procedure can also be applied without modifications to unstructured grids; however, this issue is beyond the scope of the present study).

Consider a segment of the interface located between the centre nodes of the two FV cells *i* and *j*, for which $\phi_i \le 0$ and $\phi_j > 0$ (see Fig. 2). This interface segment may be located entirely within cell *i* (as shown in Fig. 2a), entirely within cell *j*, or in both cells *i* and *j* (as shown in Fig. 2b). Denote the surface tension contributions at nodes *i* and *j,* as given by Eq. (9), as $\mathbf{B}^i_{st}$ and $\mathbf{B}^j_{st}$, respectively. In order to make the distribution of $\mathbf{B}_{st}$ less sensitive to the movement of the interface across such cell edges, $\mathbf{B}^i_{st}$ and $\mathbf{B}^j_{st}$ are replaced by distributed values, denoted by $\widetilde{\mathbf{B}}^i_{st}$ and $\widetilde{\mathbf{B}}^j_{st}$, based on the proximity of the interface to the nodes. This procedure is applied only if the angle between the normal to the interface, $\mathbf{n}$, and the normal to the edge, $\mathbf{n}_{\mathrm{ED}}$, is less than a specified value, α_S:

$$\begin{cases} \widetilde{\mathbf{B}}^i_{st} = (1-\xi)\,(\mathbf{B}^i_{st} + \mathbf{B}^j_{st}) \\ \widetilde{\mathbf{B}}^j_{st} = \xi\,(\mathbf{B}^i_{st} + \mathbf{B}^j_{st}) \end{cases} \quad \text{if } \cos^{-1}(\mathbf{n}\,\mathbf{n}_{ED}) \le \alpha_S \qquad (10)$$

where

$$\xi = \frac{V_i(F_i - 1/2) + V_j F_j}{V_i/2 + V_j/2} \quad \phi_i \le 0\,,\ \phi_j > 0, \qquad (11)$$

V_i and V_j are the respective cell volumes, and F_i and F_j are the volume fractions of the liquid phase in cells *i* and *j*. Subsequently, we refer to the Level Set formulation supplemented with the smoothing procedure defined in Eqs. (10,11) as *Modified Method B*.

In the following Sections, we examine the effect of the choice for the value of the angle α_S on the accuracy of the solution. Increasing the value of α_S increases the number of cells over which the surface tension force is distributed (Fig. 2). For instance, by setting $\alpha_S = 45^\circ$ for a square mesh, the surface tension force is distributed over all cells in a band two cells wide. From this prospective, increasing α_S renders Modified Method B analogous to Method A with $\varepsilon_\sigma = h$.

3 NUMERICAL RESULTS AND DISCUSSION

In this Section, we apply the two Level Set formulations to several selected problems, with the purpose of testing and validating the two approaches, *vis à vis*. For simplicity, all test problems are either two-dimensional or axisymmetric. In all cases, the Navier-Stokes Equations (1) are solved using second-order schemes in both space and time.

3.1 Liquid Drop at Equilibrium

As a first test, we model a drop of liquid in the absence of external forces. Ideally, the drop should acquire a spherical shape, and remain in equilibrium with a jump in pressure across the surface given by the Laplace formula:

$$\Delta p = 2\sigma / R\,, \qquad (12)$$

in which R is the radius of the drop.

We consider a drop of water of radius $R = 2\ \mathrm{cm}$ in stagnant air. The physical properties of the water are set to $\rho_L = 10^3\ \mathrm{kg/m^3}$, $\mu_L = 10^{-3}\ \mathrm{kg/m\,s}$, the water/air density and viscosity ratios are $\rho_L/\rho_G = 860$ and $\mu_L/\mu_G = 54$; the surface tension is $\sigma = 0.072\ \mathrm{N/m}$. A solution to an analogous problem, but for a planar two-dimensional drop, with $\rho_L/\rho_G = 2$, has been reported [5], but using the VOF method with a Piecewise-Constant-Stair-Stepped (PCSS) reconstruction procedure. Note the greatly increased density ratio in our case, resulting in a more challenging modelling problem.

Due to axial symmetry, the problem is modelled in cylindrical coordinates, the computational domain Ω_D representing only one half of the drop. The domain size is chosen to be $6\ \mathrm{cm} \times 3\ \mathrm{cm}$, with the air pressure at the domain external boundaries set to zero. According to the Laplace formula (12), the exact pressure distribution is $p_{exact} = 0$ outside of the drop, and $p_{exact} = p_{in}\ (= 7.2\ \mathrm{Pa})$ inside, with a discontinuous jump between the two at the drop surface.

To characterize the accuracy of the numerical solution, the following error estimates are employed:

$$E_2 = \left(\int_{\Omega_D} (p - p_{exact})^2 / (A_D\, p_{in}^2)\, d\Omega \right)^{1/2}, \qquad (13)$$

$$E_2^{in} = \left(\int_{\Omega_{in}} (p - p_{exact})^2 / (A_{in}\, p_{in}^2)\, d\Omega \right)^{1/2}, \qquad (14)$$

$$\Delta P_{rel}^{in} = \int_{\Omega_{in}} (p - p_{exact}) / (A_{in}\, p_{in})\, d\Omega\,. \qquad (15)$$

The first two are calculated in the L_2 norm, while the last quantifies the error in calculating the pressure inside the drop. Here, Ω_{in} is the part of Ω_D for which the volume fraction of water, F_L, satisfies the condition: $F_L(\mathbf{x}) \ge 0.99$. Correspondingly, A_D and A_{in} are the cross-sectional areas of regions Ω_D and Ω_{in}. The errors defined by Eqs. (14,15) were introduced by

Table 1: Convergence study of the two Level Set methods: the density and viscosity are smoothed across the computational interface, with smoothing parameters $\varepsilon = 2h$, as defined in Eqs. (4,5).

h/R	Error	Method A		Method B	Modified Method B		
		$\varepsilon_\sigma = h$	$\varepsilon_\sigma = 2h$		$\alpha_s = 10^\circ$	$\alpha_s = 15^\circ$	$\alpha_s = 20^\circ$
0.05	E_2	$7.03\cdot10^{-2}$	$8.34\cdot10^{-2}$	$7.33\cdot10^{-2}$	$7.65\cdot10^{-2}$	$7.61\cdot10^{-2}$	$7.70\cdot10^{-2}$
	E_2^{in}	$4.36\cdot10^{-3}$	$3.72\cdot10^{-3}$	$7.59\cdot10^{-3}$	$6.94\cdot10^{-3}$	$8.47\cdot10^{-3}$	$1.01\cdot10^{-2}$
	ΔP_{rel}^{in}	$3.94\cdot10^{-3}$	$1.26\cdot10^{-3}$	$6.46\cdot10^{-3}$	$5.28\cdot10^{-3}$	$7.43\cdot10^{-3}$	$8.91\cdot10^{-3}$
0.025	E_2	$5.11\cdot10^{-2}$	$6.00\cdot10^{-2}$	$5.31\cdot10^{-2}$	$5.39\cdot10^{-2}$	$5.44\cdot10^{-2}$	$5.48\cdot10^{-2}$
	E_2^{in}	$1.95\cdot10^{-3}$	$2.36\cdot10^{-3}$	$6.99\cdot10^{-3}$	$5.30\cdot10^{-3}$	$5.54\cdot10^{-3}$	$4.96\cdot10^{-3}$
	ΔP_{rel}^{in}	$1.42\cdot10^{-3}$	$3.59\cdot10^{-4}$	$-6.03\cdot10^{-3}$	$-4.62\cdot10^{-3}$	$-4.73\cdot10^{-3}$	$-3.81\cdot10^{-3}$

Brackbill *et al.* [5], and we adopt them here for comparison purposes.

Table 1 shows the results of the convergence study. We note that, in terms of the E_2 error, all Level Set formulations exhibit slower than first-order convergence; this is to be expected, since the exact solution to the problem is discontinuous. In terms of the E_2^{in} error, Method A displays first-order convergence for both values of ε_σ, while the two-fold reduction in mesh size results in approximately a three-fold reduction in pressure error, ΔP_{rel}^{in}. Modified Method B has a similar convergence rate to that of Method A for the values $\alpha_s = 15^\circ$ and 20°, but quite slow convergence for $\alpha_s = 10^\circ$. Method B has the slowest convergence characteristics of all the methods considered. In general, we note that the use of Method A results in smaller errors E_2^{in} and ΔP_{rel}^{in} compared with Method B and Modified Method B. On the other hand, comparison of the results listed in Table 1 with those obtained by Brackbill *et al.* [5], shows that each of the Level Set methods yields a level of accuracy one order of magnitude higher than that of the PCSS VOF method.

3.2 Zero-Gravity Drop Oscillation

We now consider small oscillations of a two-dimensional, planar drop around its equilibrium shape in an infinite, gaseous medium, in the absence of gravity. If we consider only the fundamental mode of oscillation, an analytical solution to the linearized problem, which can be used to represent the exact solution in the case of small oscillations, can be found in Lamb [13]. According to this solution, the position of the interface of a drop of radius R, oscillating at its fundamental mode, is given, in polar coordinates (r,θ), by:

$$\frac{r(\theta,t)}{R} = 1 + \tilde{\varepsilon}\cos(2\theta)\cos(\omega_d t)\exp(-t/\tau_d), \quad (16)$$

where $\tilde{\varepsilon}$ is the initial perturbation of the drop, and ω_d and τ_d are the frequency and characteristic time of decay due to viscous damping, respectively:

$$\omega_d^2 = \frac{6\sigma}{R^3(\rho_L + \rho_G)} \quad , \quad \tau_d = \frac{R^2}{4}\frac{(\rho_L + \rho_G)}{(\mu_L + 3\mu_G)}, \quad (17)$$

while the combined kinetic energy of the drop and surrounding gas is given by

$$K_T(t) = \frac{\pi}{4}(\rho_L + \rho_G)\tilde{\varepsilon}^2 R^2 \omega_d^2 \sin^2(\omega_d t)\exp(-2t/\tau_d). \quad (18)$$

For the numerical simulation, we choose the problem configuration studied before by other groups: namely, the Essentially non-Oscillatory (ENO) Level Set method [10] and the front-tracking method [1]. Thus, the characteristic length is set to $l_c = R$, and the Reynolds and Weber numbers to $Re = 20$ and $We = 2$, respectively. The density and viscosity ratios are set to $\rho_L/\rho_G = 100$ and $\mu_L/\mu_G = 100$, and the characteristic velocity is correspondingly given by

$$u_c = \frac{\sigma}{\mu_L}\frac{We}{Re}.$$

The interface $r(\theta,0)$ of the drop at $t = 0$ is initialized with $\tilde{\varepsilon} = 0.05$, as defined in Eq. (16).

Due to symmetry, it is only necessary to solve the problem in the half-domain (scaling according to Eq. 1c),

$$\Omega^* = \left\{(x^*, y^*) \,\middle|\, 0 \le x^* \le 4,\ 0 \le y^* \le 2\right\},$$

in which the centre of gravity of the drop is located at (2,0). A free-slip boundary condition is imposed along the symmetry line, and constant pressure is imposed on the rest of the domain boundary. The simulations are performed using a structured, rectangular grid of resolution 200×100, and with time step $\Delta t^* = 0.01$.

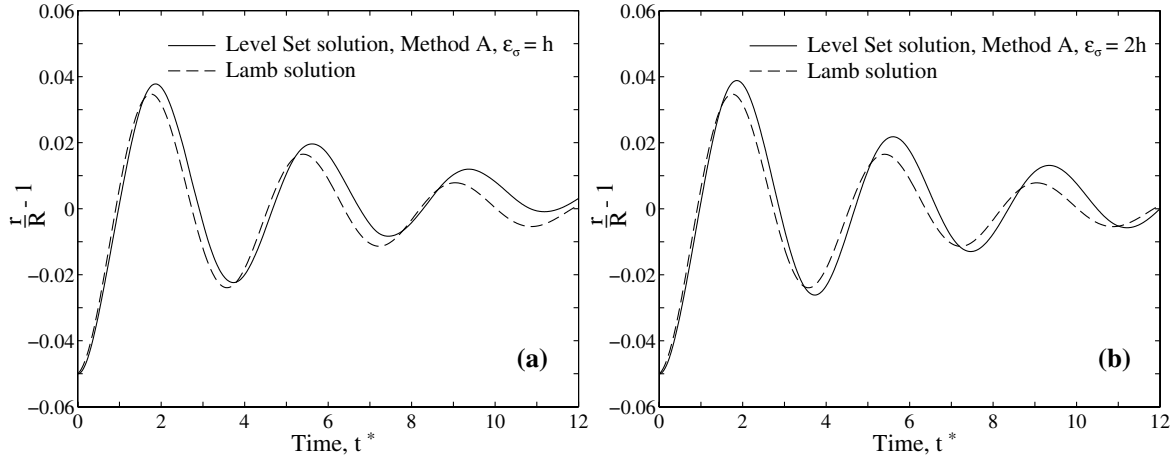

Fig. 3: Time evolution of the point $r^*(\pi/2, t^*)$ on the interface of the oscillating two-dimensional drop, as predicted by Method A: (a) $\varepsilon_\sigma = h$; (b) $\varepsilon_\sigma = 2h$. The dashed line shows the analytical solution of the linearized problem. The properties of the fluid are: $\rho_L / \rho_G = 100$, $\mu_L / \mu_G = 100$, $Re = 20$, $We = 2$.

Figure 3 shows the displacement of the interface at $\theta = \pi/2$ as a function of time, as given by the analytical and Level Set solutions. Method A has been employed with two different values of ε_σ (h and $2h$), and both are seen to give similar, and reasonably accurate, solutions. In the case $\varepsilon_\sigma = h$, the solution displays a clear, gradual shift of the equilibrium position away from the line $r/R - 1 = 0$. We believe that this numerical artefact is caused by increase of mass of the drop during the simulation, as well as parasitic currents developing near the interface (to be discussed in the next Section). Similarly, but less noticeably, this shift can also be seen in the solution of the axisymmetric oscillating-drop problem obtained reported elsewhere [10,14], both obtained using the ENO Level Set Method. In our solution, the shift is more noticeable for the case $\varepsilon_\sigma = h$, although the solution obtained using $\varepsilon_\sigma = 2h$ appears to have a larger amplitude error. Figure 4 shows the total kinetic energy, K_T^*, and the relative mass of the drop versus time for the two simulations.

Evidently, the larger amplitude error observed in the solution obtained using $\varepsilon_\sigma = 2h$ may be explained by the fact that, in this case, the kinetic energy is somewhat overestimated. In terms of energy conservation, use of the parameter $\varepsilon_\sigma = h$ appears to give a solution closer to the analytical solution.

However, as Fig. 4b indicates, the case $\varepsilon_\sigma = 2h$ results in better mass conservation than for $\varepsilon_\sigma = h$. The displacement of the interface at $\theta = \pi/2$ as a function of time, obtained using Method B (both the original and modified formulations), is shown in Fig. 5. As can be seen, the unmodified Method B gives completely the wrong solution, while the accuracy of the solution obtained using Modified Method B depends on the value of the sector angle α_S: the larger the value of α_S, the higher the accuracy. For instance, the value $\alpha_S = 20^\circ$ (Fig. 5d) seems to produce a solution of comparable accuracy to that of Method A with $\varepsilon_\sigma = h$ (Fig. 3a).

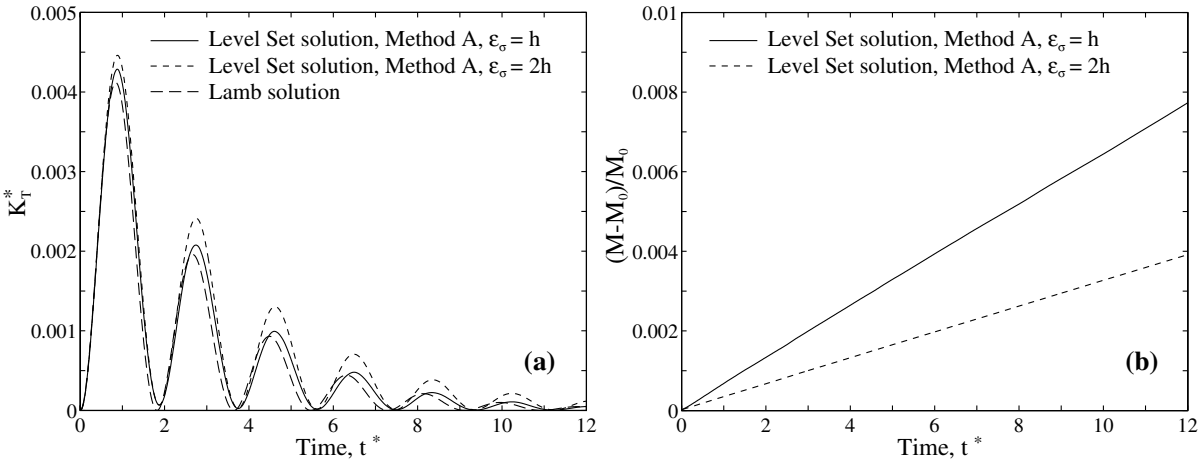

Fig. 4: Solutions of the oscillating two-dimensional drop problem produced by Method A for $\varepsilon_\sigma = h$ and $\varepsilon_\sigma = 2h$: (a) total kinetic energy of the flow vs. time; (b) fractional variation of the mass of the drop vs. time.

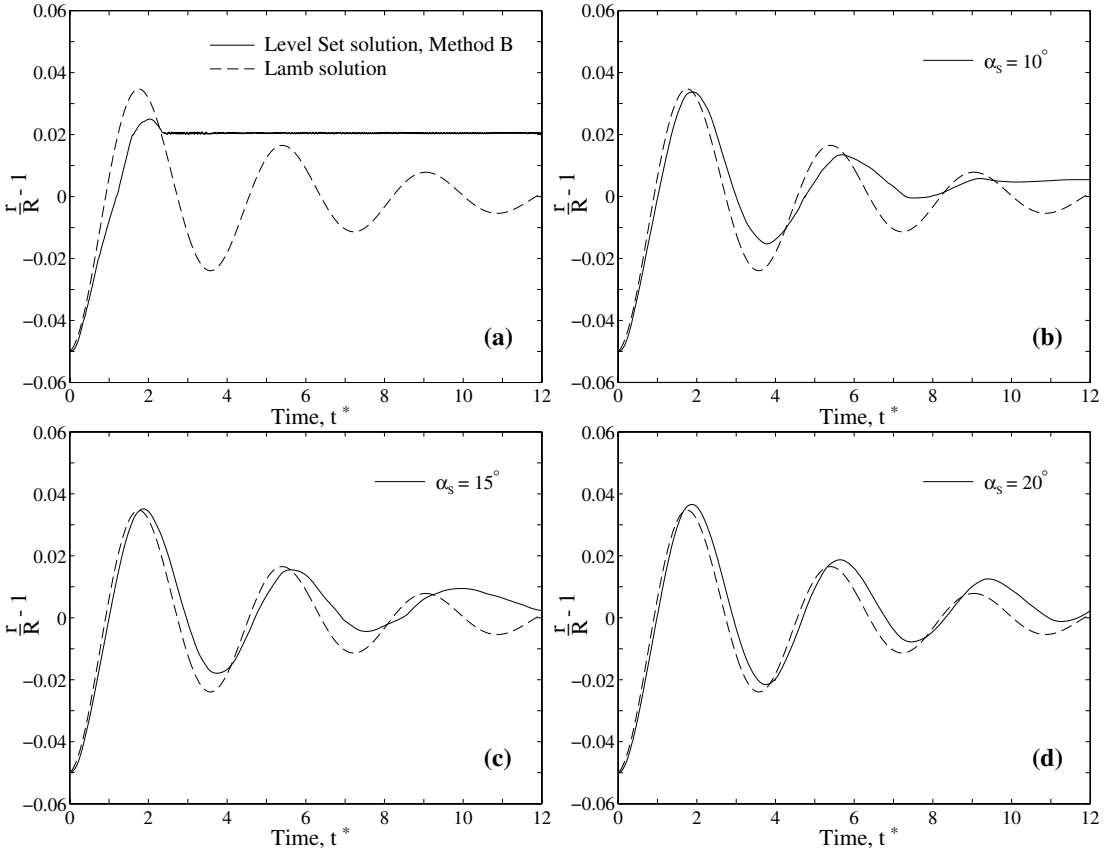

Fig. 5: Displacement of the interface of the oscillating two-dimensional drop, $r^*(\pi/2, t^*)$, as predicted by: (a) Method B; and Modified Method B with (b) $\alpha_S = 10^\circ$, (c) $\alpha_S = 15^\circ$, (d) $\alpha_S = 20^\circ$.

Figure 6 shows the kinetic energy of the flow, K_T^*, as a function of time for both Method B and Modified Method B. Evidently, of the four cases considered, only Modified Method B with $\alpha_S = 20^\circ$ seems to provide good conservation of energy, whereas the other solutions display unacceptable levels of damping.

In terms of mass conservation, both the original Method B and its modified version display practically identical properties as those of Method A with $\varepsilon_\sigma = h$. The mass of the drop grows almost linearly with time (c.f. Fig. 4b), and at time $t^* = 12$ (about three cycles), the relative increase in the mass of the drop is about 0.8%, and is independent of the value of α_S.

To summarize, as demonstrated for the stationary and oscillating drop problems, Method B can fail, or produce erroneous solutions, in situations in which the surface tension is the main driving force of the flow. In order to improve accuracy, the method needs to be modified with some smoothing procedures, replacing the localized representation of the surface-tension force with one that distributes the force around the interface. Our Modified Method B is an example of such a method.

3.3 Parasitic Currents

Parasitic currents are unphysical flows developing around phase interfaces as a result of a local imbalance in the normal pressure and the shear stresses, as a result of discretization errors [15]. These currents are known to have an adverse effect on performance of numerical interface-tracking algorithms, particularly when the flow configuration is close to equilibrium and there are strong surface-tension forces [15].

In order to compare the intensities of the parasitic flows developing for the two surface tension models considered here, we simulate a static, planar drop of liquid, with zero initial disturbance. This problem has received much attention in the literature [15,16]. Theoretically, if such a drop is placed in a stagnant, gaseous medium, in the absence of gravity, the drop and the surrounding medium should remain motionless. In a numerical simulation, however, this does not happen, due to parasitic currents developing around the interface. Consequently, it becomes important to control and minimize their amplitude and rate of growth. For the simulation reported here, we adopt a problem configuration identical to that used in the previous Section for the oscillating drop, except that the initial disturbance, $\tilde{\varepsilon}$, is set to zero.

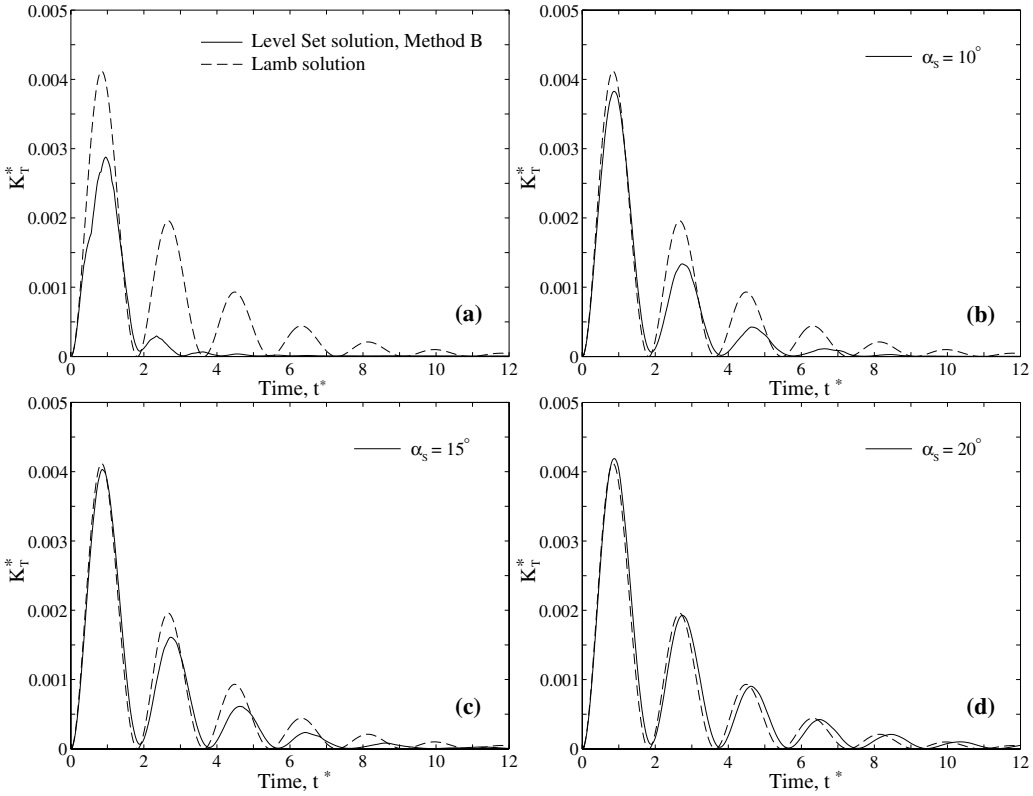

Fig. 6: Total kinetic energy, K_T^* vs. time of the oscillating two-dimensional drop, as predicted by: (a) Method B, and Modified Method B with (b) $\alpha_S = 10^\circ$, (c) $\alpha_S = 15^\circ$ and (d) $\alpha_S = 20^\circ$.

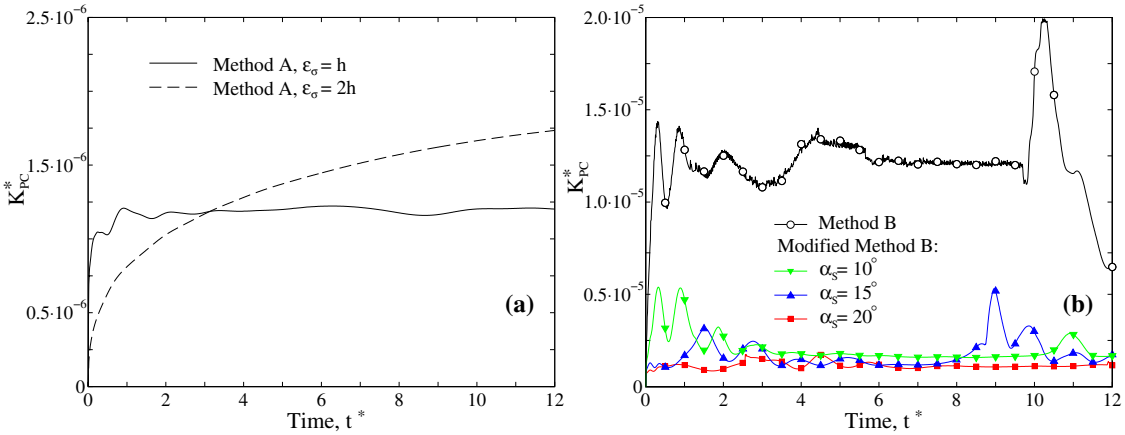

Fig. 7: Kinetic energy of the parasitic currents in the problem of a static drop in zero gravity: (a) Method A; (b) Method B and Modified Method B. The properties of the liquid are: ρ_L / ρ_G = 100, μ_L / μ_G = 100, *Re* = 20, *We* =2

Figure 7 shows the total kinetic energy of the parasitic currents, defined as:

$$K_{PC}^* = \int_{\Omega^*} \tfrac{1}{2} \rho^* u^{*2} \, d\Omega^* .$$

The relationship between the physical and scaled variables is as given in Eq. (1c). We note that for the solutions obtained using Method A, the scale of K_{PC}^* is approximately the same for both $\varepsilon_\sigma = h$ and $\varepsilon_\sigma = 2h$, for the time interval $0 \le t^* \le 12$. The intensity of the parasitic currents observed in simulations carried out using Modified Method B appears to depend on the value of α_S employed (see Fig.7b). The value $\alpha_S = 20^\circ$ yields the lowest average level for K_{PC}^*, and is close to that obtained using Method A with $\varepsilon_\sigma = h$. The standard Method B gives the highest (by one order of magnitude) value of the K_{PC}^*.

Another common measure of the intensity of the parasitic currents is the maximum velocity $u_{\max}^*$ observed in the computational domain during the simulation [15,16]. We found that, for the present problem, the value of $u_{\max}^*(t^*)$ in the time interval $0 \le t^* \le 12$ produced by Method A, both for $\varepsilon_\sigma = h$ and $\varepsilon_\sigma = 2h$, rapidly reach maximum values of 0.02, and 0.028 respectively, but thereafter remain

constant. In contrast, the functions $u^*_{\max}(t^*)$ for Modified Method B oscillate slightly around an average value of ≈ 0.03 for each of the cases $\alpha_S = 10^\circ$, 15° and 20°. For the standard Method B, $u^*_{\max}$ is highly oscillatory, with an average value of 0.1, and local maxima as high as 0.22.

To summarize, Method B (concentrated surface tension force) appears to be highly susceptible to parasitic currents. Though adaptation is possible (Modified Method B), there are no clear advantages over Method A, which treats the surface tension force in a distributed manner.

3.4 Gas Bubble Rising in a Viscous Fluid

For this simulation, we use data from the experiment conducted by Hnat and Buckmaster [17], who examined terminal topologies of air bubbles rising in mineral oil. The density and viscosity of the oil are $\rho_L = 876\,\mathrm{kg/m^3}$ and $\mu_L = 0.118\,\mathrm{kg/m\,s}$, giving oil/air density and viscosity ratios as follows: $\rho_L / \rho_G = 714$ and $\mu_L / \mu_G = 6670$; the surface tension is $\sigma = 0.032\,\mathrm{N/m}$. Though experimental data are available for bubbles of different sizes, we model here bubbles of the smallest volume ($V_b = 0.94\,\mathrm{cm^3}$),for which the surface-tension effects are the strongest.

Initially, at $t = 0$, the bubble is approximated as a sphere of radius $r_b = 0.61\,\mathrm{cm}$. We non-dimensionalize the problem by setting the distance and velocity scales to $l_c = r_b$ and $u_c = U_t^{exp}$ (See Eq. 1c), where $U_t^{\exp}$ is the experimental terminal rise velocity of the bubble. The following dimensionless groups: $Re = 9.8$, $Fr = 0.76$, and $We = 7.6$. Since the problem is axisymmetric, we model only half of the bubble. The computational domain chosen for the simulation is $\Omega^* = \{(r^*, z^*) \mid 0 \le r^* \le 4.9, 0 \le z^* \le 20\}$, where r^* and z^* are radial and vertical coordinates. At $t = 0$, the centre of mass of the bubble is at $(r^*, z^*) = (0,4)$. At the sides of Ω^*, except the symmetry line at $r^* = 0$, a far-field boundary condition is employed, according to which the fluid pressure is set to $p = \rho_L g z$.

Calculations have been performed with mesh resolution $h^* = 0.05$, and time step $\Delta t^* = 0.01$. Surprisingly, all Level Set formulations employed for this simulation displayed robust convergence and almost identical bubble shapes. This can be seen in Fig. 8, which shows the bubble cross-sections at different times for each model. The bubble achieves steady state after $t^* = 8$, corresponding to a physical time of approximately 0.22 s. The terminal bubble rise velocities and aspect ratios (the ratio of bubble width to height) are given in Table 2. In addition, Fig. 9a shows the position of the centre of mass of the bubble, z_c^*, versus time, obtained using Method A (with $\varepsilon_\sigma = 2h$) and Method B. (The other methods predict almost identical behaviour, and are therefore not shown in the Figure.) In terms of mass conservation, both Method B and Modified Method B seem to yield slightly better results compared to Method A, as seen in Fig. 9b.

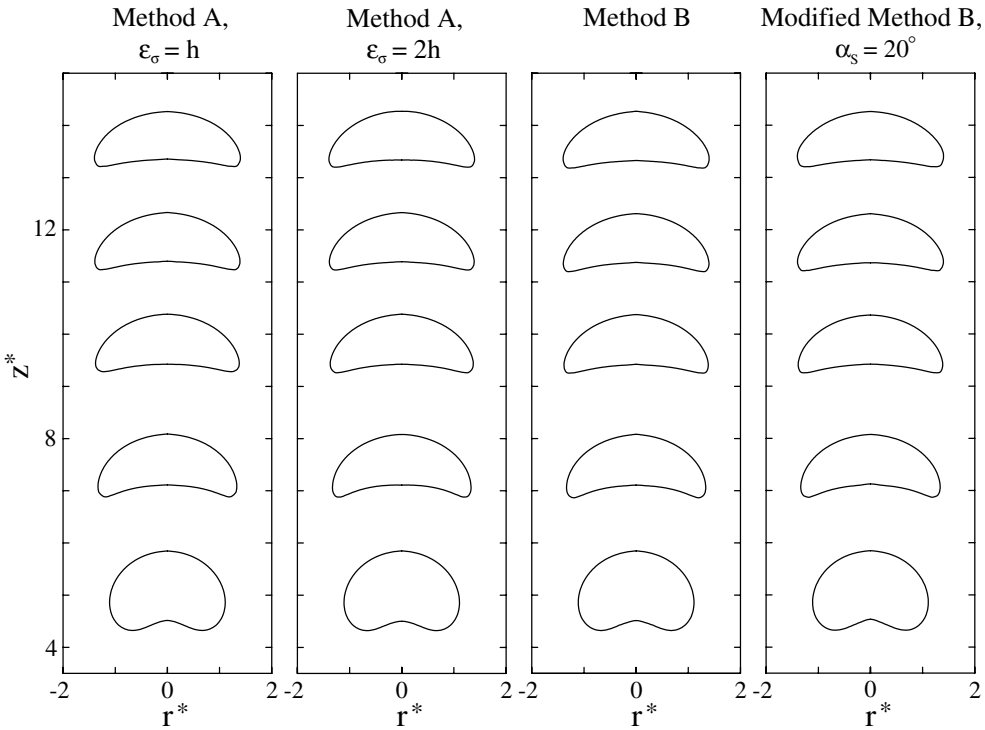

Fig. 8: Evolution of an air bubble in mineral oil, as predicted by the different Level Set formulations: Method A, ε_σ = h; Method A, ε_σ = 2h; Method B; and Modified Method B, with α_s = 20. Cross-sections of the bubble are shown at times t* = 1.2, 3.6, 6.0, 8.0, 10.0. The distance and time scales are l_c = 0.61 cm and t_c = 0.028 s.

Table 2: Terminal rise velocity, U_t, and aspect ratio, w_b / l_b, of a fully-developed, spherical-cap air bubble in oil. The experimental data were obtained by Hnat and Buckmaster [17].

Results	Experiment	Method A		Method B	Modified Method B
		$\varepsilon_\sigma = h$	$\varepsilon_\sigma = 2h$		$\alpha_S = 20^\circ$
U_t (cm/s)	21.5	21.1	21.1	21.2	21.3
w_b / l_b	2.7	2.7	2.6	2.6	2.7

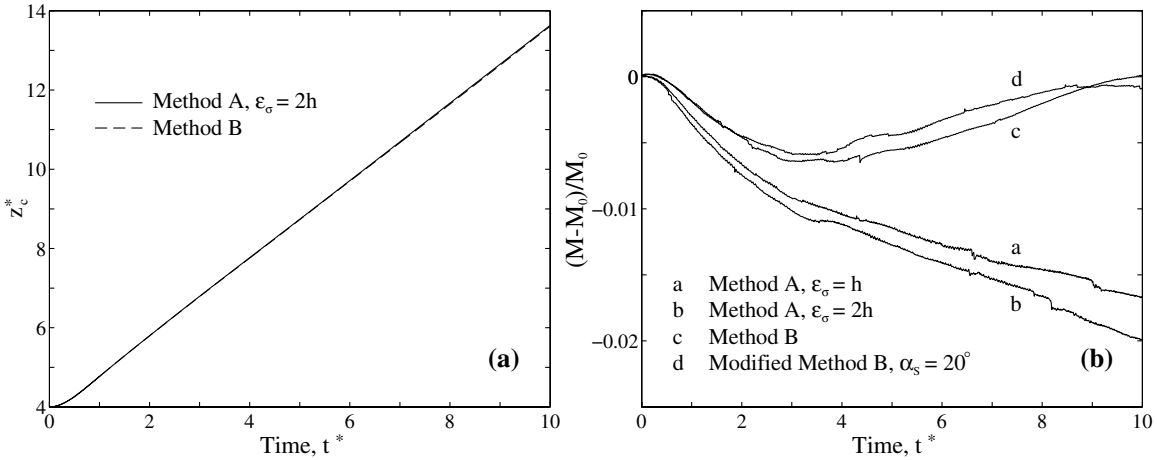

Fig. 9: Level Set solutions for the problem of a rising air bubble in oil: (a) position of the centre of mass, z_c^*, vs. time; (b) relative bubble mass vs. time.

4 CONCLUSIONS

We have analyzed two surface-tension models for simulating incompressible, viscous, two-phase flows with moving interfaces. Both models have been incorporated into a hybrid Finite-Element/Finite-Volume Level Set interface-tracking formulation, comprising a Finite-Element treatment of the equations governing the motion of the interface, and a Finite-Volume solution of the Navier-Stokes equations. The FE/FV Level Set method has been implemented into the commercial CFD code CFX-4.

The first model (referred to in the text as *Method A*) is based on a traditional Level Set approach, in which the surface-tension is distributed over a band of computational cells around the interface using a smoothed Delta function. The second model (referred to as *Method B*) employs the integral form of fluid/flow equations, and the surface tension force is imposed only in those computational cells which the interface traverses. This second model has been successfully used before by Ilic *et al*. [9] in the context of a VOF approach, but, to our knowledge, it has never been applied in combination with the Level Set method.

We have considered several applications for which surface tension effects are prevalent: (a) a static, spherical drop in the absence of external forces; (b) an oscillating drop of liquid in a gaseous medium; (c) parasitic currents around a drop of liquid in gas; and (d) an air bubble rising in a viscous fluid. These studies have revealed that Method A always produces satisfactory results, while Method B displays rather slow convergence for application (a), gives a completely erroneous solution for application (b), and produces the highest intensity of parasitic currents in application (c). In application (d), both Methods A and B have been found to perform equaly well.

It has also been demonstrated that, in order to make Method B robust and more accurate, it is necessary to introduce a smoothing procedure. We have demonstrated that by redistributing the surface tension force locally in a band, two computational cells wide. By doing so, the accuracy of the method can be improved significantly. However, this modification makes Method B virtually analogous to Method A.

The success of Ilic *et al*. [9] in using a concentrated surface-tension model analogous to Method B for rising bubbles has been seen also in the present work, though we have used much higher density and viscosity ratios. However, the work here indicates that in other situations the method is less satisfactory than traditional, distributed approaches. Thus, summarizing the observations noted above, we conclude that Method A, traditional to the Level Set community, is the more general, and more robust procedure. Use of Method B can be successful in applications in which surface-tension effects are not dominant, but generally the method is not robust, and does not bring any particular advantages to interfacial flow modelling in the context of the Level Set approach.

REFERENCES

[1] G. Tryggvason,, B. Bunner, A. Esmaeeli, D. Juric, N. Al-Rawahi, W. Tauber, J. Han, S. Nas, Y.-J. Jan, "A Front-Tracking Method for the Computations of Multiphase Flow", *J. Comput. Phys.*, **169**, 708-759 (2001).

[2] T.Y. Hou, J.S. Lowengrub, M.J. Shelley, "Boundary integral methods for multi-component fluids and multiphase materials", *J. Comput. Phys.*, **169**, 302-323 (2001).

[3] D. Jacqmin, "Calculation of Two-Phase Navier-Stokes Flows Using Phase-Field Modelling", *J. Comput. Phys.*, **155**, 96-127 (1999).

[4] D. Jamet, O. Lebaigue, N. Coutris, J.M. Delhaye, "The Second Gradient Method for the Direct Numerical Simulation of Liquid-Vapor Flows with Phase Change", *J. Comput. Phys.*, **169**, 624-651 (2001).

[5] J.U. Brackbill, D.B. Kothe, C. Zemach, "A Continuum Method for Modelling Surface Tension", *J. Comput. Phys.,* **100**, 335-354 (1992).

[6] J.A. Sethian, *Level Set Methods and Fast Marching Methods: Evolving Interfaces in Computational Geometry, Fluid Mechanics, Computer Vision, and Materials Science,* Cambridge University Press, 1999.

[7] T.J. Barth, J.A. Sethian, "Numerical Schemes for the Hamilton-Jacobi and Level Set Equations on Triangulated Domains", *J. Comput. Phys.,* **145**, 1-40 (1998).

[8] M. Sussman, E.G. Puckett, "A Coupled Level Set and Volume-of-Fluid Method for Computing 3D and Axisymmetric Incompressible Two-Phase Flows". *J. Comput. Phys*., **162**, 301-337 (2000).

[9] M. Ilic, M. Wörner, D.G. Cacuci, "Balance of Liquid-Phase Turbulence Kinetic Energy Equation for Bubble-Train Flow". *J. Nucl. Sci. Technology,* **41**, 331-338 (2004).

[10] M. Sussman, P. Smereka, S. Osher, "A Level Set Approach for Computing Solutions to Incompressible Two-Phase Flow", *J. Comput. Phys.,* **114**, 146-159 (1994).

[11] M. Sussman, E. Fatemi, "An Efficient Interface-Preserving Level Set Redistancing Algorithm and its Application to Interfacial Incompressible Fluid Flow", *SIAM J. Sci. Comput*., **20**, 1165-1191 (1999).

[12] S.V. Shepel, B.L. Smith, S. Paolucci, "Implementation of a Level Set Interface Tracking Method in the FIDAP and CFX-4 Codes", Proc. 5th ASME/JSME International Symposium on Computational Technologies for Fluid/Thermal/Chemical/ Stressed Systems with Industrial Applications, PVP-Vol.491-2, 31-41 San Diego, USA, July 25-29, 2004.

[13] H. Lamb, *Hydrodynamics,* Dover 1945.

[14] M. Sussman, P. Smereka, "Axisymmetric free boundary problems", *J. Fluid Mech.,* **341**, 269-294 (1997).

[15] B. Lafaurie, C. Nardone, R. Scardovelli, S. Zaleski, G. Zanetti, "Modelling Merging and Fragmentation in Multiphase Flows with SURFER", *J. Comput. Phys.,* **113**, 134-147 (1994).

[16] S. Popinet, S. Zaleski, "A Front-Tracking Algorithm for Accurate Representation of Surface Tension", *Int. J. Numer. Meth. Fluids,* **30**, 775-793 (1999).

[17] J.G. Hnat, J.D. Buckmaster, "Spherical Cap Bubbles and Skirt Formation", *Phys. Fluids*, **19**, 182-194 (1976).